Journal of Power Sources 255 (2014) 9–15

Contents lists available at ScienceDirect

Journal of Power Sources

journal homepage: www.elsevier.com/locate/jpowsour

Experimental study of a passive thermal management system for high-powered lithium ion batteries using porous metal foam saturated with phase change materials

W.Q. Li, Z.G. Qu*, Y.L. He, Y.B. Tao

State Key Laboratory of Multiphase Flow in Power Engineering, Energy and Power Engineering School, Xi'an Jiaotong University, Xi'an, Shaanxi 710049, China

HIGHLIGHTS

- Cooling structure for Li-ion battery using foam-paraffin composite was designed.
- Thermal management by air natural convection cannot fulfill battery safety demand.
- Employment of pure PCM dramatically reduced battery surface temperature.
- Integration of copper foam and paraffin further reduced battery temperature.
- Battery surface temperature increased with increase in porosity and pore density.

ARTICLE INFO

Article history:
Received 12 October 2013
Received in revised form
11 December 2013
Accepted 1 January 2014
Available online 8 January 2014

Keywords:
Thermal management
Lithium ion battery
Metal foam
Phase change materials

ABSTRACT

A highly efficient thermal strategy to manage a high-powered Li-ion battery package within the required safe temperature range is of great demand for electric vehicles (EVs) applications. A sandwiched cooling structure using copper metal foam saturated with phase change materials was designed. The thermal efficiency of the system was experimentally evaluated and compared with two control cases: a cooling mode with pure phase change materials and an air-cooling mode. The results showed that the thermal management with air natural convection cannot fulfill the safety demand of the Li-ion battery. The use of pure PCM can dramatically reduce the surface temperature and maintain the temperature within an allowable range due to the latent heat absorption and the natural convection of the melted PCM during the melting process. The foam-paraffin composite further reduced the battery's surface temperature and improved the uniformity of the temperature distribution caused by the improvement of the effective thermal conductivity. Additionally, the battery surface temperature increased with an increase in the porosity and the pore density of the metal foam.

1. Introduction

Lithium-ion batteries are generally treated as substitutes for nickel metal batteries and lead acid batteries for use in hybrid electric vehicles (HEVs) or electric vehicles (EVs) due to their high power density, stable charge and discharge cycle and relatively long lifespan. These large scale batteries are packed in series or in parallel in some applications that have a greater power demand, and, in this case, the battery temperature during the charge and discharge process must be maintained within an allowable temperature range when using this integrated package to avoid thermal runaway situations due to excessively high (greater than 60 °C) or extremely low temperatures (below 0 °C), which can decrease the battery lifetime, as stated in Refs. [1,2]. Additionally, the temperature uniformity among various cells was demonstrated to be crucial to the battery pack's safety because large temperature differences can cause the capacity of the entire battery pack to decrease [3]. Therefore, a very efficient temperature regulation and thermal management system is necessary for a high-powered Li-ion battery module.

A variety of heat dissipation techniques and designs have been previously reported in the literature. Wu et al. [4] designed a self-contained heat pipe attached to the battery surface to mitigate the temperature increase during discharge and found that the addition of the heat pipe combined with air forced convection reduced the rate of temperature increase and resulted in a more

* Corresponding author. Tel./fax: +86 029 82668036.
E-mail address: zgqu@mail.xjtu.edu.cn (Z.G. Qu).

0378-7753/$ – see front matter © 2014 Elsevier B.V. All rights reserved.
http://dx.doi.org/10.1016/j.jpowsour.2014.01.006

uniform temperature distribution. Pesoaran [5] designed a liquid-based thermal management system for batteries in EV applications and measured the battery temperature during the discharge process. The results demonstrated that the cooling efficiency was significantly improved using a liquid-based cooling system. Nelson et al. [6] modeled and compared the thermal control systems for lithium batteries based on an air-cooled and a fluid-cooled method. Their results demonstrated that the transfer fluid was superior to air for cooling the battery. Fan et al. [7] numerically analyzed the thermal behavior of prismatic lithium ion cells within an air-cooled module. They found that reducing the gap between the cells or increasing the velocity of the air resulted in a decrease in the temperature increase.

The thermal efficiency is improved with active thermal management of forced air convection and liquid cooling; however, additional structural complexity or an extra cost associated with the energy supply was required. In the past decades, a thermal management system using organic PCM was preferred. The organic PCM offers advantages of greater latent heat, stable chemical characteristics, a proper phase change temperature and a reasonable price [8]. Sabbah et al. [9] compared the effectiveness of two dissipation modes using air forced air convection and phase change materials under the same discharge condition for 1.5 Ah 18650 commercial batteries. Their experimental results revealed that the PCM cooling system resulted in a better thermal performance compared with the active air at a discharge rate of 1.3C with a stressful 40 °C ambient temperature. Duan and Naterer [10] experimentally investigated a thermal management technique for a lithium ion battery using phase change materials. Their results demonstrated that the battery temperature was reduced to a safe temperature range by means of the PCM. Although PCMs are excellent candidates for thermal storage and management applications, the intrinsic and undesirably low thermal conductivity of most organic PCMs has, to a large extent, restricted their thermal applications in high-energy charge/discharge rate systems [11]. Confronted with this challenge, various solutions to improve the effective thermal conductivity of PCMs have been proposed. Fan and Khodadadi [12] conducted experimental and theoretical studies into thermal conductivity enhancement technologies, including adding extended fins, inserting high thermal conductivity particles and using a porous metallic medium. In EV applications, Kizilel et al. [13] reported that PCMs in combination with expanded graphite outperformed the active air-cooling system at various discharge rates under extreme ambient conditions. Khateeb et al. [14] experimentally investigated four dissipation modes for a 2.2 Ah 18650 cell package and demonstrated that the use of aluminum foam/PCM composite presented an additional decrease in the temperature increase of approximately 5 °C compared with the pure PCM. An efficient cooling technique of encapsulating a PCM with copper metal foam was studied by Li et al. [15]. The experimental results demonstrated that the use of the metal foam can dramatically improve the effective thermal conductivity of the PCM and reduce the surface temperature of the heater.

From a review of the literature, studies investigating the thermal management of high-powered batteries using foam-PCM composites have been inadequate. Additionally, the effects of the geometric parameters of the metal foam on the thermal performance of the batteries are rarely mentioned in previous studies. In this study, a passive thermal dissipation system for high-energy $Li_yMn_2O_4$ batteries using the integration of a metallic copper foam and a PCM was designed. Two additional thermal dissipation modes, including air natural convection and a pure PCM, were also used as reference cases. The thermal behaviors of the system were evaluated by comparing the battery's surface temperature using the three dissipation modes described above. The effects of the morphology parameters of the metal foam were also investigated.

2. Thermal properties of the PCM and the metal foam

Commercial paraffin (RT 44HC) was employed as the organic PCM. The fusion point, the specific heat capacity and the heat of the paraffin were measured using a Differential Scanning Calorimeter (DSC, TA-Q20, USA). The paraffin sample was heated from 20 °C to 80 °C at a rate of 5 °C min^{-1}. Fig. 1 shows the testing results. The fusion point is from 42.76 °C to 49.24 °C, and the latent heat is 270.7 J g^{-1}. The remaining thermal properties are shown in Table 1. Fig. 2 shows the local morphology of the copper foam supplied by ChangSha Lyrun Material Co., Ltd., China. Five foam samples with different porosities (ε) and pore densities (ω, PPI: pore number per inch) were used in the experiment. The effective thermal conductivity (k_e) can be theoretically determined using Eqs. (1)–(4) in Ref. [16]. The geometric parameters and the thermal dynamic properties are shown in Table 2.

$$k_e = \frac{1}{\sqrt{2}(R_A + R_B + R_C + R_D)} \tag{1}$$

$$R_A = \frac{4\lambda}{[2e^2 + \pi\lambda(1-e)]k_s + [4 - 2e^2 - \pi\lambda(1-e)]k_f} \tag{2}$$

$$R_B = \frac{(e-2\lambda)^2}{(e-2\lambda)e^2k_s + [2e - 4\lambda - (e-2\lambda)e^2]k_f} \tag{3}$$

$$R_C = \frac{\left(\sqrt{2}-2e\right)^2}{2\pi\lambda^2\left(1-2\sqrt{2}e\right)k_s + 2\left[\sqrt{2}-2e-\pi\lambda^2\left(1-2\sqrt{2}e\right)\right]k_f} \tag{4}$$

3. Experimental setup and procedure

Fig. 3 shows the experimental system that consists of three modules: the test section, the charge/discharge module and the data acquisition system. The copper foam-paraffin composite was prepared by infiltrating the liquid paraffin into the pores of the metal foam in a hot water bath. Fig. 4(a) shows the thermal management of the foam-paraffin composite; the battery pack was formed by organizing ten of the foam-paraffin plates and nine of the Li-ion cells with 10 Ah capacity in the pattern of a compact

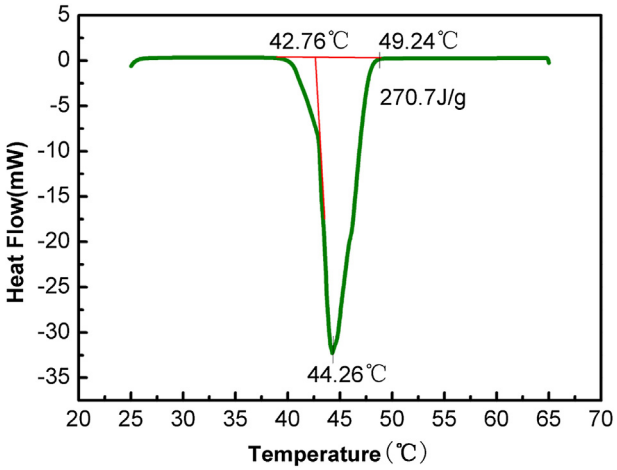

Fig. 1. DSC testing results for the paraffin.

Table 1
Thermophysical properties of paraffin.

Parameters	Value
Density (g cm^{-3})	810
Latent heat (kJ kg^{-1})	270.7
Specific heat capacity (J kg^{-1} K^{-1})	2250
Thermal conductivity (W m^{-1} K^{-1})	0.2
Kinematic viscosity (m^2 s^{-1})	4.4×10^{-3}

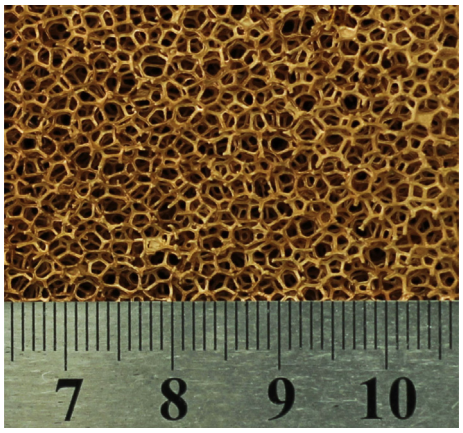

Fig. 2. Local morphology of the metal foam ($\omega = 20$ PPI).

sandwich structure. The batteries were assembled in a series connection. To quantitatively describe the effect of the metal foam, one additional thermal management pattern using the pure PCM was also designed with a similar configuration, as shown in Fig. 4(b). Additionally, the batteries were simply assembled in a series connection to demonstrate another reference case using air natural convection. The details of the battery properties provided by the battery manufacturer are listed in Table 3.

The battery pack was charged and discharged using an Innet Battery Cycler (model: DCLT-4805TL, Taiwan) with an accuracy of ±1% in the constant current mode. During the charging process, the battery pack was charged at a constant 0.5C rate. During the discharge period, the battery pack was tested under three separate discharging rates: 0.5C, 1C and 3C. A total of 9 T-type thermocouples (Omega Engineering Inc., USA) with an accuracy of ±0.1 °C were used to track the battery surface temperature. Each thermocouple was mounted on the middle of each battery surface because the battery was considered to present a uniform temperature distribution. The ambient temperature of the laboratory was maintained with control and another thermocouple was used to track the ambient temperature near the battery pack which was around 25 °C(±1 °C) during the experiment. During a typical cycle, the battery was charged at an initial temperature of approximately 25 °C. After the charge process was completed, the battery pack was naturally cooled to the ambient temperature. Then, the battery pack was discharged at the specified rate and cooled again to a steady state temperature. The batteries' surface temperatures were obtained every 30 s and tracked using the Agilent data acquisition system (34970A, USA).

Table 2
Geometric and thermophysical properties of the foam-paraffin composites.

Parameters	Sample no.				
	S-1	S-2	S-3	S-4	S-5
Porosity, ε	0.90	0.95	0.97	0.97	0.97
Pore density, ω, (PPI)	20	20	20	10	40
k_e, (W m^{-1} K^{-1}) [16]	11.33	6.35	0.80	0.80	0.80

4. Results and discussion

4.1. Cooling using air natural convection

Fig. 5 shows the temperature history with time for a whole charge and discharge cycle for the battery pack at two locations (cell-5 and cell-9, as shown in Fig. 4) at the 0.5C and 1C discharge rates. During the charge process ($\tau < 95$ min), the two temperature curves increased until arriving at a maximum value of 42 °C for cell-5 and 37 °C for cell-9 at the end of charge. During the discharge period (205 min $< \tau <$ 265 min), the temperature for cell-5 increased by 43 °C to reach 68 °C at the end of the discharge, which exceeded the battery safety temperature (65 °C). This dramatic temperature increase is due to the low convective heat transfer coefficient of air natural convection and the suppression of the air motion in such an integrated battery module. This undesirable temperature increase demonstrates that passive thermal cooling using air natural convection has the potential to expose the battery to a disastrous situation and endanger the battery's life, especially in extreme environmental conditions. Additionally, the surface temperature difference between the two cells was greater than 10 °C. Dickinson and Swan reported in Ref. [17] that the non-uniformity in the temperature distribution in a cell pack increased the chance of capacity fade of the battery system. Therefore, large temperature differences within a cell pack are not desirable.

4.2. Cooling using the pure PCM

Fig. 6 shows the surface temperature variations with time for the thermal management case using the pure PCM at the same charge and discharge conditions as that of air natural convection (Fig. 5). In the charge process ($\tau < 95$ min), the maximum temperatures at the end of the charge for cell-5 and cell-9 were 33 °C and 30 °C, which were 9 °C and 7 °C less, respectively, compared with temperatures from the previous case without the PCM. The temperature at this stage did not reach the melting temperature of the PCM and no melting phenomenon occurred. This phenomenon implies that the heat dissipation efficiency via thermal conduction of the paraffin was greater than that of the natural convection of the air during the charge process. When the temperature first increased from the ambient temperature (25 °C) to the melting point of the paraffin (42 °C) during the discharge process (175 min $< \tau <$ 230 min), the temperature increase rate declined because the solid paraffin began to melt and the heat was stored as the latent heat of the PCM at the solid/liquid interface. At the end of the discharge stage, the maximum temperatures of cell-5 and cell-9 were 53 °C and 47 °C, respectively, which were less than the safety temperature (65 °C). During the cooling period after the discharge process (230 min $< \tau <$ 465 min), the temperature first underwent a sharp temperature drop to the melting point and then decreased smoothly due to the release of the latent heat during the solidification until the temperature approached the onset melting temperature. Then, the temperature decrease rate increased again because the explicit heat release prevailed. Therefore, the time consumption for the pure PCM was twice as much as in the case of air natural convection (Fig. 5) due to the latent heat release.

4.3. Cooling using the copper foam-paraffin composite

Because the temperature during the charge process is much less than the battery safety temperature, the surface temperature during the discharge process is only discussed in this section. Fig. 7

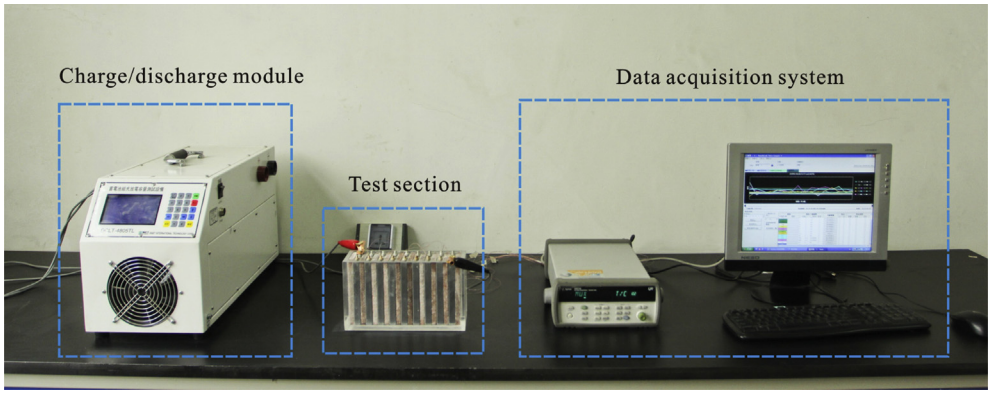

Fig. 3. Experimental setup.

shows the surface temperature responses for the cases of the air natural convection, the pure PCM and the foam-paraffin composite ($\varepsilon = 0.97$, $\omega = 40$ PPI) at discharge rates of 0.5C, 1C and 3C. The initial temperature was approximately 25 °C. During the 0.5C discharge process, as seen in Fig. 7(a), the temperature for the three cases increased in an almost linear manner. The maximum temperature for the air convection case reached 48 °C at the end of discharge. Comparatively, the maximum temperatures were 41 °C and 40 °C for the pure PCM and foam-PCM composite, respectively. This result indicates that the paraffin remained as a solid phase during the discharge rate of 0.5C, which leads to the conclusion that thermal conduction was the dominant heat transfer mechanism. As seen in Table 3, the effective thermal conductivity of the foam-paraffin composite (0.82 W m^{-1} K^{-1}) was greater than that of the pure PCM (0.3 W m^{-1} K^{-1}), which resulted in the lowest temperature among the three cases; however, the temperature of the foam-PCM composite was slightly less than that of the pure PCM because contact thermal resistance existed between the foam and the battery surfaces.

For the battery pack undergoing the three dissipation modes at a 1C discharge rate, the comparison results of the battery surface temperatures are shown in Fig. 7(b). The temperature for the air natural convection was the greatest among the three cases, and a maximum temperature of 70 °C was obtained for the air natural convection case. This greatest temperature exceeded the safety temperature of the battery (65 °C). In comparison, the PCM melted in the case of the pure PCM and the foam-PCM composite at this discharge rate. The discharge period can be divided into three regions: solid, melting and liquid. In the solid region, where the surface temperatures were below the melting point, the foam-paraffin composite resulted in a lower surface temperature level than that of the pure PCM due to the enhanced effective thermal conductivity caused by the foam. The time consumption to the onset melting temperature (τ_1) for the foam-paraffin composite was correspondingly longer than that for the pure PCM (τ_0). During the melting process, the solid paraffin transformed to a liquid phase, and the considerable latent heat was stored at the moving solid–liquid interface, and natural convection occurred that was attributed to the buoyancy force of the melted paraffin. The combined heat conduction and natural convection of the melted paraffin exerted their roles during the melting process for the composite material. Consequently, the effect of the heat conduction was greater than that of the natural convection, which caused the surface temperature for the foam-paraffin composite to increase at

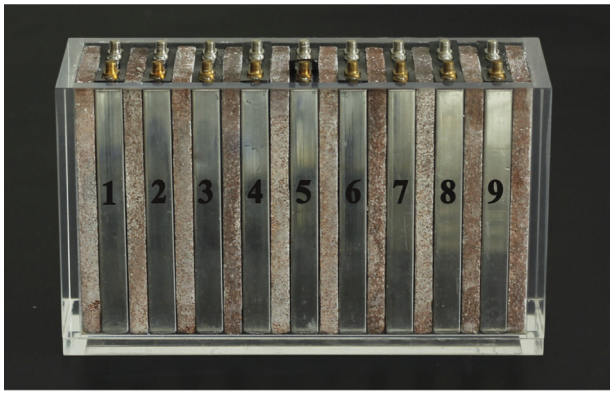

(a)

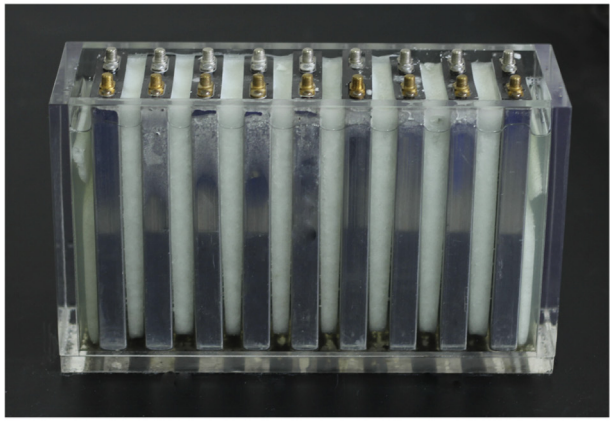

(b)

Fig. 4. Battery pack design (a) using the copper foam-paraffin composite and (b) pure PCM.

Table 3
Electrical characteristics of the Li-ion cell.[a]

Parameters	Value
Capacity (Ah)	10
Length (mm)	140
Width (mm)	65
Thickness (mm)	15
Nominal voltage (V)	3.8
Cell pack voltage (V)	34.2
Cut-off voltage (V)	4.65
Maximum discharge current (A)	30 (3C)

[a] Provided by the battery manufacturer.

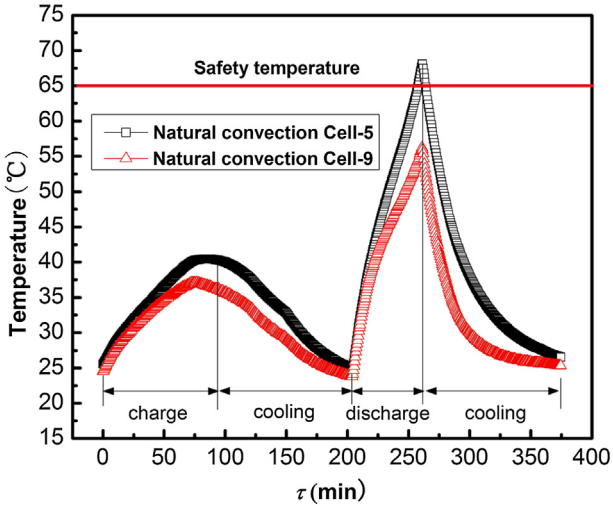

Fig. 5. Temperature variations with time for the air natural convection for the 1C discharge rate.

a relatively slow rate and remain at a lower level within the melting temperature range compared with the pure PCM. In the liquid stage, only the explicit heat was absorbed for both the pure PCM and the foam-paraffin composite. At the end of the discharge, the surface temperature of the foam-paraffin composite decreased by 29% and 12% compared with the surface temperature of the air convection and the pure PCM, respectively.

Fig. 7(c) shows the surface temperature as a function of time for the three cases for the 3C discharge rate. The temperature curves were similar to those shown in Fig. 7(b). The experiment was intermittent because the temperature for the air natural convection dramatically increased to 80 °C during the 13th minute of the discharge process. The addition of the foam structure to the paraffin reduced the surface temperature by almost 6 °C at the expense of the shortened thermal management time ($\Delta\tau_1$), compared with the temperature for the pure PCM ($\Delta\tau_2$), due to the reduced total quantity of latent heat absorption in the composite material. Although the battery surface temperature did not exceed the limited point of 65 °C for the pure PCM and the foam-paraffin composite after the melting process, the temperature increases were almost 8 °C within 2 min for the former case and 10 °C within

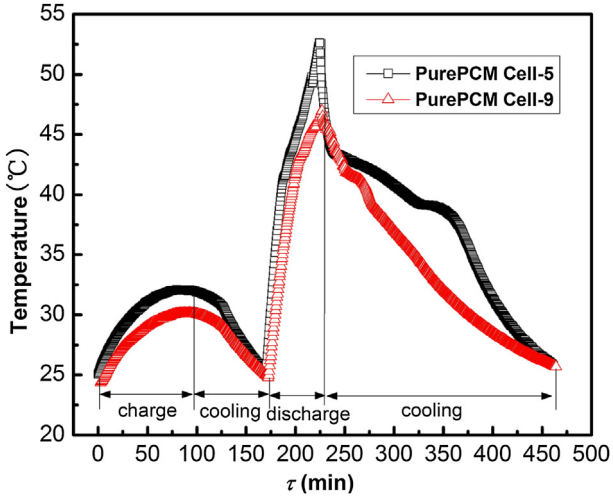

Fig. 6. Temperature variations with time for the pure PCM for the 1C discharge rate.

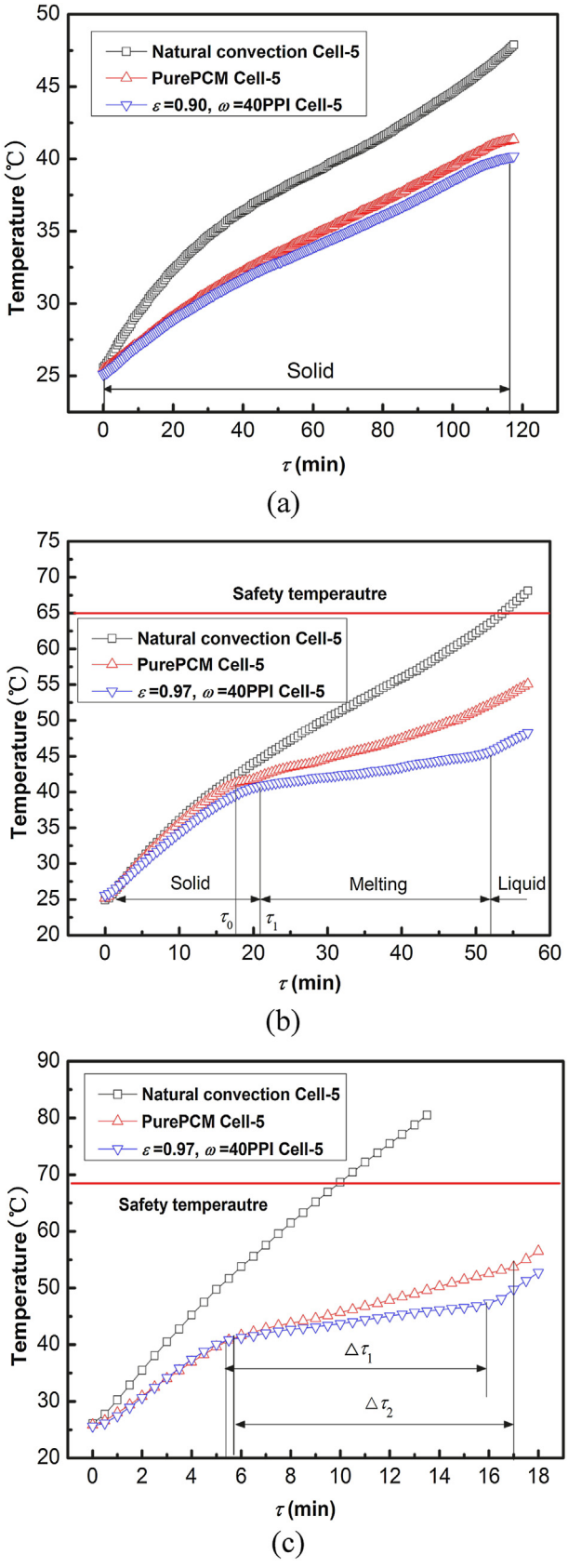

Fig. 7. Temperature variations with time under three dissipation modes (a) for the 0.5C discharge rate; (b) for the 1C discharge rate; and (c) for the 3C discharge rate.

3 min for the latter case. These dramatic increases in the surface temperature created a potential threat to the battery safety at this high discharge rate. This situation can be avoided by enlarging the gap between two adjacent batteries to accommodate for a greater amount of PCM.

Fig. 8 shows the temperature history with time in the same charge and discharge cycle that is shown in Figs. 5 and 6. The maximum temperature difference between cell-5 and cell-9 in the battery pack for the foam-paraffin composite at the end of discharge was approximately 4 °C, which is significantly less than the difference observed during the air convection mode (Fig. 5) and when using the pure PCM (Fig. 6). This small temperature gradient in the battery pack indicated that the impregnation of the PCM into the metal foam can effectively improve the uniformity of the temperature distribution in the battery pack.

4.4. Effect of foam porosity

Fig. 9 shows the effect of foam porosity ($\varepsilon = 0.90, 0.95, 0.97$) on the surface temperature of cell-3 under a fixed pore density of 20 PPI for the 1C discharge rate. The effective thermal conductivity, which can be calculated using Eqs. (1)–(4), is negatively related with the foam porosity. The effective thermal conductivity of the foam-paraffin composite samples with porosities of 0.90, 0.95 and 0.97 are 11.33, 6.35 and 0.80 W m^{-1} K^{-1}, respectively. The interfacial surface area ratio is defined using the expression in Eqs. (5) and (6) from Ref. [18]:

$$a_{sf} = \frac{3\pi d_f}{d_p^2} \tag{5}$$

$$d_f = 1.18\sqrt{\frac{1-\varepsilon}{3\pi}}\left[\frac{d_p}{1-e^{-(1-\varepsilon)/0.04}}\right] \tag{6}$$

The interfacial area increases with a decrease in the porosity. The improved effective thermal conductivity and the extended surface area in the lower porosity samples can play a positive role in reducing the battery's surface temperature. Conversely, the natural convection of the melted paraffin was significantly constrained in the sample with the lower porosity, and this suppression did not reduce the surface temperature. The positive factors on the effective thermal conduction and the interfacial heat transfer were more dominant than the negative suppression of the natural convection

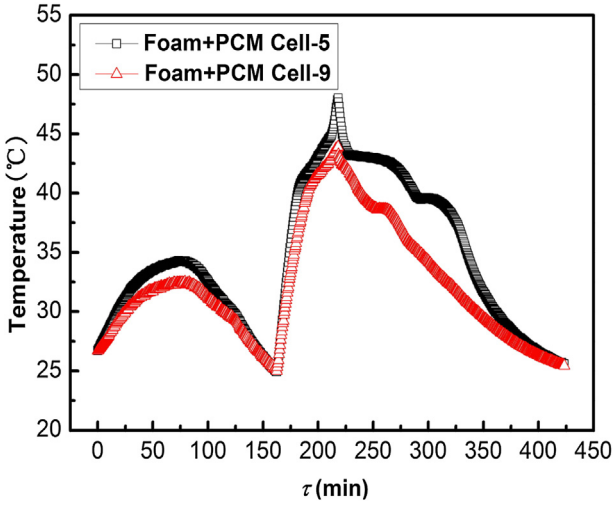

Fig. 8. Temperature variations with time for the foam-paraffin composite for the 1C discharge rate.

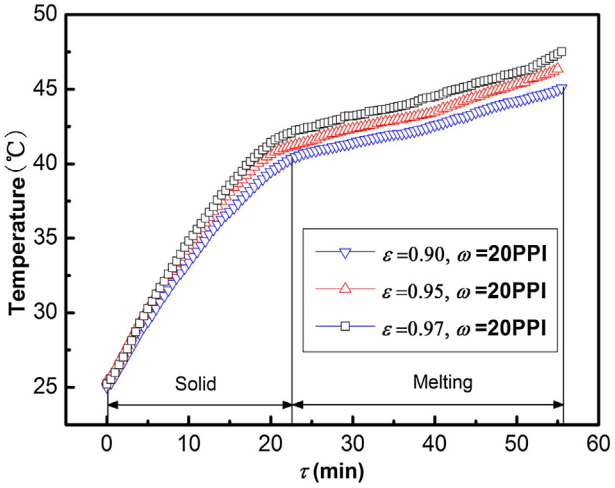

Fig. 9. Effect of the porosity on the battery temperature of cell-3 for the 1C discharge rate.

of the melted paraffin [15]. Therefore, the temperature for the lowest porosity sample ($\varepsilon = 0.90$) resulted in the lowest temperature among the three samples during the melting process.

4.5. Effect of pore density

The effect of the pore density ($\omega = 10$, 20, and 40 PPI) on the temperature history of cell-4 at a fixed porosity of 0.97 for the 1C discharge is shown in Fig. 10. The battery surface temperature for the sample with the 40 PPI density resulted in the greatest temperature. The effective thermal conductivity is primarily dependent on the porosity, as defined in Eqs. (1)–(4). The effective thermal conductivities for the three samples were identical for the fixed porosity due to having the same fraction of the metallic matrix and the PCM. Therefore, the heat transfer process was dominated by the interfacial heat transfer and the natural convection of the liquid paraffin. Conversely, the permeability of the porous structure decreased with an increase in the pore density, as stated in Ref. [19]; thus, the natural convection of the melted paraffin was most significantly suppressed for the sample with the greatest pore density (40 PPI). Conversely, the interfacial area ratio increased with an increase in the pore density, which demonstrates that the

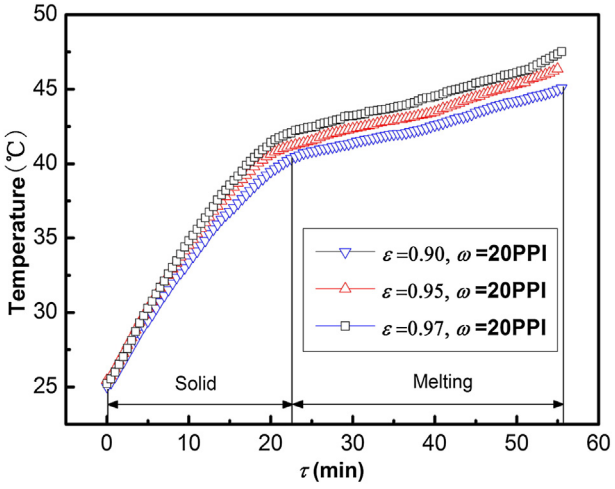

Fig. 10. Effect of the pore density on the battery temperature of cell-4 for the 1C discharge rate.

sample with the greatest pore density (40 PPI) has the greatest surface area. Consequently, the effect of the permeability was more dominant than the interfacial heat transfer inside the foam, which resulted in the highest temperature for the most compact structure ($\omega = 40$ PPI).

5. Conclusion

A passive thermal management system for high powered lithium-ion battery packs using a sandwich structure combined with copper foam saturated with paraffin was designed and experimentally investigated. The battery temperature using air convection cooling exceeded the safety limit. The paraffin remained in a solid state for the lower discharge rate of 0.5C. Melting of the PCM occurred at the greater 1C and 3C discharge rates, and the temperatures were less than the safety temperature for both the pure PCM and the foam-PCM composite. The discharge process was correspondingly classified into three regions: solid, melting and liquid. The foam-PCM composite resulted in the lowest battery temperature and most uniform temperature distribution in the cell pack, followed by the pure PCM. The battery surface temperature was reduced with decreased porosity at a fixed pore density due to the dominant effect of the heat conduction and the surface area. The battery surface temperature also increased with increased pore density due to the dominant effect of the permeability.

Acknowledgments

The authors appreciate the support of the National Excellent Doctoral Dissertation Foundation of China (201041), National Key Basic Research Program of China (973 Project: 2011CB610306), Fok Ying Tung Education Foundation of China (131054), and the National Natural Science Foundation of China (No. 51322604).

References

[1] R.B. Wright, J.P. Christophersen, C.G. Motloch, J.R. Belt, C.D. Ho, V.S. Battaglia, J.A. Barnes, T.Q. Duong, R.A. Sutula, J. Power Sources 119–121 (2003) 865–869.
[2] P. Ramadass, B. Haran, R. White, B.N. Popov, J. Power Sources 112 (2002) 614–620.
[3] R. Kizilel, A. Lateef, R. Sabbah, M.M. Farid, J.R. Selman, S. Al-Hallaj, J. Power Sources 183 (2008) 370–375.
[4] M.S. Wu, K.H. Liu, Y.Y. Wang, C.C. Wan, J. Power Sources 109 (2002) 160–166.
[5] A.A. Pesaran, in: Proceedings of Advanced Automotive Battery Conference, USA, 6–8February, 2001.
[6] P. Nelson, D. Dees, K. Amine, G. Henriksen, J. Power Sources 110 (2002) 349–356.
[7] L. Fan, J.M. Khodadadi, A.A. Pesaran, J. Power Sources 238 (2013) 301–312.
[8] F. Agyenim, N. Hewitt, P. Eames, M. Smyth, Renewable Sustainable Energy Rev. 14 (2010) 615–628.
[9] R. Sabbah, R. Kizilel, J.R. Selman, S. Al-Hallaj, J. Power Sources 182 (2008) 630–638.
[10] X. Duan, G.F. Naterer, Int. J. Heat Mass Transfer 53 (2010) 5176–5182.
[11] M.M. Farid, A.M. Khudhair, S.A. Razack, S. Al-Hallaj, Energy Convers. Manage. 45 (2004) 1597–1615.
[12] L. Fan, J.M. Khodadadi, Renewable Sustainable Energy Rev. 15 (2011) 24–46.
[13] R. Kizilel, R. Sabbah, J.R. Selman, S. Al-Hallaj, J. Power Sources 194 (2009) 1105–1112.
[14] S.A. Khateeb, S. Amiruddin, M. Farid, J.R. Selman, S. Al-Hallaj, J. Power Sources 142 (2005) 345–353.
[15] W.Q. Li, Z.G. Qu, Y.L. He, W.Q. Tao, Appl. Therm. Eng. 37 (2012) 1–9.
[16] K. Boomsma, D. Poulikakos, Int. J. Heat Mass Transfer 44 (2001) 827–836.
[17] B. Dickinson, D. Swan, in: Proceedings of the Future Transportation Technology Conference and Exposition, USA, 1995.
[18] V.V. Calmidi, R.L. Mahajan, J. Heat Transfer 122 (2000) 557–565.
[19] J.G. Fouriea, J.P. Du Plessis, Chem. Eng. Sci. 57 (2002) 2781–2789.